

Highly Sensitive Electrochemical Biosensor Assembled by Au Nanoparticle /MOF-5 Composite Electrode for DNA Detection

Huimin Yang^{1,*}, Lingjun Han², Jing Liu¹, Yupeng Li¹, Dingding Zhang¹, Xian Liu², Zhenhai Liang^{1,*}

¹ College of Chemistry and Chemical Engineering, Taiyuan University of Technology, Taiyuan 030024, PR China

² Department of Chemistry, Taiyuan Normal University, Jinzhong 030619, PR China

*E-mail: yanghuimin@tyut.edu.cn, liangzhenhai@tyut.edu.cn, liangzhenh@sina.com

Received: 3 February 2019 / Accepted: 4 April 2019 / Published: 10 May 2019

An efficient and sensitive electrochemical method for detecting trace amounts of sequence-specific deoxyribonucleic acid (DNA) by using a gold nanoparticle (Au NP)/metal–organic framework (MOF) composite electrode was developed. An electrochemical DNA sensor was constructed by introducing Au NPs as electrochemical signal labels to an MOF-5-modified glassy carbon electrode as the adsorption background platform. The unique porous structural characteristics of MOF-5 considerably enhanced the electrocatalytic activity of the Au NPs and improved the DNA detection limit of the resultant electrode. The cyclic voltammetry, linear sweep voltammetry, and chronoamperometry results for the electrochemical DNA sensor demonstrated that the electro-oxidation current gradually increased as the target DNA concentration was increased. Target DNA concentrations of 1 pM to 100 nM presented a good linear relationship with current. The calculated detection limit was 0.05 pM. The Au/MOF composite electrode materials presented considerable potential for application in the development of electrochemical biosensors for DNA detection.

Keywords: Metal-organic framework; electrochemical sensor; DNA; Gold nanoparticles; electrocatalytic oxidation

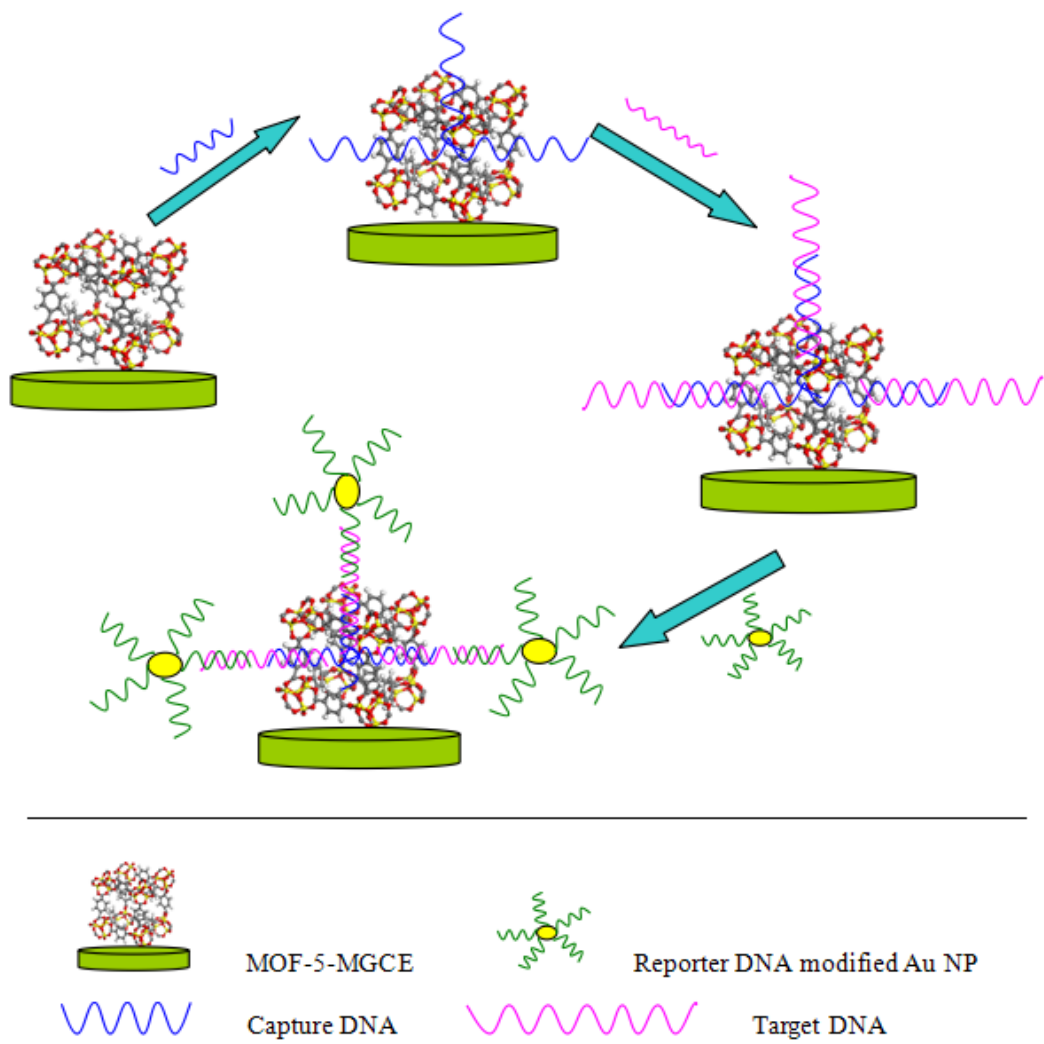
1. INTRODUCTION

The sensitive, rapid, and low-cost detection of biomolecules even at low concentrations is crucial for clinical diagnostic and therapeutic applications. Deoxyribonucleic acid (DNA) is one of the most important genetic materials in vivo. DNA can be detected by using numerous methods, such as gel electrophoresis and chemiluminescent[1], biotin–avidin[2], and fluorescent[3] labeling methods. These methods, however, present either radiological hazards or low sensitivity. Electrochemical biosensors

demonstrate multiple advantages, such as rapidity, high selectivity and sensitivity, and low cost, and can be applied to perform on-line continuous monitoring even in complex systems[4]. Patterson[5] developed a reagent-less electrochemical biosensor for the detection of double-stranded DNA by using a triplex-forming oligonucleotide as the probe. Its integrated, miniaturized, and highly automated features have facilitated its extensive use in clinical genetic disease control, environmental testing, and legal identification.

Classical DNA detection is based on the hybridization of complementary single-stranded DNA with other DNA strands[6]. DNA electrochemical biosensors are mainly composed of single-stranded DNA molecules anchored to an electrode and an electrocatalytic active substance. Metal nanoparticles can enhance electron transfer rates and reduce over-potentials during oxidation and reduction[7]. Gold nanoparticles (Au NPs) have been used to fabricate various types of modified electrodes because of their good biocompatibility, large surface area, high conductivity, renewable surfaces, and excellent electrocatalytic activity. They can effectively overcome the drawbacks of radioisotope, enzyme, and fluorescence markers when used as markers for DNA detection[8]. Au NPs can form strong covalent Au–S bonds with mercapto groups and combine with amino groups through strong noncovalent electrostatic adsorption. Gold sol and bioactive molecules can combine to form probes through the above effects. Zhu[9] reported on a Au NP-based colorimetric assay for detecting single-nucleotide polymorphisms in triple-stranded DNA. Bard[10] exploited the current amplification that occurs when a platinum NP collides with and adheres to an inert electrode and that results in a rapid electrocatalytic reaction. Au NPs can enhance and amplify signals during electrochemical detection and improve sensor sensitivity. Therefore, Au NPs are excellent electrochemical signal labels for biosensors. In electrochemical studies, metal NPs are immobilized on an inert supporting material to form an electrode, and their effect on electrocatalytic reactions, such as proton or oxygen reduction, is probed. For example, the catalysis of hydrazine oxidation by Au NPs can be denoted as a detection reaction response to electrocatalytic activity.

Metal–organic frameworks (MOFs) are highly crystalline inorganic–organic hybrids constructed by assembling metal ions with multidentate organic ligands via coordinate bonding. MOFs have emerged in recent years as promising materials for molecular recognition, magnetism, photoluminescence, gas storage, drug delivery, and heterogeneous catalysis because of their flexibility, porosity, large surface areas, and well-defined configurations[11-13]. Several groups have reported novel strategies for applying MOFs in the colorimetric detection of glucose[14], cytidine triphosphate, and adenosine 5'-triphosphate[15] and have preliminarily introduced MIL-101 as a fluorescence anisotropy amplifier for DNA detection[16]. Chen first utilized MOF as a fluorescence quenching platform for DNA assays and thrombin analysis[17]. Zhu and coworkers demonstrated that MOFs can be used as a sensing platform for HIV DNA and for thrombin detection[18]. However, reports on the use of MOFs with Au NPs for electrochemical DNA detection are scarce. Ligands in MOFs usually contain a conjugated π -electron system that allows binding with DNA molecules[19]. MOF pores can act as hosts that carry other materials into cells. These aspects render MOFs as optimal supporting materials that, when combined with Au NPs, can form a composite electrode that enables DNA detection.



Scheme 1. Schematic illustration of stepwise assembly of Au/MOF-5-composite electrode electrochemical DNA sensor

In the present study, MOF-5($Zn_4O(BDC)_3$; BDC = 1,4-benzene-dicarboxylate), a cationic MOF, was employed as a supporting material for Au NPs. The coordination center was Zn^{2+} , and the bridging ligand was terephthalic acid. Terephthalic acid conjugates the π -electron system for DNA binding. MOF-5 presents strong affinity for negatively charged DNA through π - π stacking and electrostatic interactions. We attempted to demonstrate the potential use of a Au NP/MOF-5 composite electrode for DNA detection and obtain electrochemical DNA biosensor responses by catalyzing the electro-oxidation of hydrazine. The electrochemical DNA sensor was assembled as illustrated in Scheme 1. The MOF-5–MGCE bound to the captured DNA as a result of hydrophobic and π -stacking interactions between nucleobases and MOF-5[20]. Hybridization with the target DNA then occurred in accordance with complementary base-pairing rules and was succeeded by further hybridization with the reporter-DNA-modified Au NPs and the formation of a stable sandwich-type bioelectrode. Electrochemical DNA biosensor responses were obtained through the catalyzed electro-oxidation reaction of hydrazine. This design method is simple, easy to operate, highly sensitive, inexpensive, and practical.

2. EXPERIMENTAL

2.1 Reagents and apparatus

All reagents were of analytical reagent grade and used as purchased without further purification. DNA samples were purchased from Sangon Bioengineering (China). The DNA sequences were as follows: capture probe, SH-5'-GAT GATG ACG TTC CTT-3'; reporter probe, SH-5'-TCT TGG CTG TCC CAA TCC AAA-3'; target DNA, 5'-TTT GGA TTG GGA CAG CGC AAG GAA CGT CATC-3'; one base-mismatched DNA, 5'-TTT GTA TTG GGA CAG CGC AAG GAA CGT CATC-3'; three base-mismatched DNA, 5'-TTT GGA CCA GGA CAG CGC AAG GAA CGT CATC-3'; non-complementary DNA, 5'-CGC TAC AAT TTT AGA AGC AAG GAA CGT CATC-3'. Capture and reporter probes deviated with thiol groups at the 5' phosphate end. Pregnant liquor concentrations of $100 \mu\text{mol}\cdot\text{L}^{-1}$ DNA were used. The phosphate buffer solution ($50 \text{ mmol}\cdot\text{L}^{-1}$, pH=7) was composed of $\text{Na}_2\text{HPO}_4\cdot 12\text{H}_2\text{O}$ and $\text{NaH}_2\text{PO}_4\cdot 2\text{H}_2\text{O}$. The electrolyte was the $50 \text{ mmol}\cdot\text{L}^{-1}$ phosphate buffer solution containing 16mM hydrazine hydrate.

Scanning electron microscopy (SEM) micrographs were acquired using a JSM-7001F system (Jeol, Japan). Transmission electron microscopy (TEM) images were obtained using a JEM-2100 equipment (Jeol, Japan). Cyclic voltammetry (CV) and linear sweep voltammetry (LSV) were performed on a CHI660D electrochemical workstation (CH Instruments, USA). The prepared DNA sensor was used as the working electrode, Pt wire was selected as the auxiliary electrode and Ag/AgCl electrode was used as the reference electrode.

2.2 Synthesis of MOF-5 and Au NPs

The electrosynthesis procedure performed in this work was based on our previously reported method[21] with minor modifications. In this work, we selected 1-butyl-3-methylimidazolium chloride as the ionic liquid. The characterization results for the prepared MOF-5 are provided in the Supporting Information.

All vessels used in this step were cleaned by using freshly prepared aqua regia and then rinsed with copious amounts of double-distilled water (ddH₂O). An 18.5 mL aliquot of ultrapure water was placed in a beaker and then mixed with 0.5 mL of $1.0 \times 10^{-2} \text{ mol}\cdot\text{L}^{-1}$ chloroauric acid solution followed by 0.5 mL of $1.0 \times 10^{-2} \text{ mol}\cdot\text{L}^{-1}$ potassium citrate solution. Subsequently, 0.5 mL of $0.1 \text{ mol}\cdot\text{L}^{-1}$ sodium borohydride was added to the mixture after 5 min of rapid stirring and dispersion through magnetic stirring. The stirring rate was then reduced, and Au sol was successfully obtained at a concentration of $2.5 \times 10^{-4} \text{ mol}\cdot\text{L}^{-1}$ after 10 min of continuous stirring. The Au sol was finally transferred to a brown bottle. The UV-vis spectra of the prepared Au NPs are shown in the Supporting Information section.

2.3 Preparation of MOF-5 modified glassy carbon electrode

Prior to electrode modification, a GCE (3 mm diameter) was polished by applying alumina slurry with a polishing cloth. The GCE was then placed in acetone, nitric acid solution (V HNO₃:V H₂O = 1:1), and ddH₂O and ultrasonicated for 10 min. A stable suspension containing 40 mg of MOF-5, 20 mg of

carbon black, 2 mL of ethanol, and 1 mL of ddH₂O was prepared through 30 min of ultrasonic agitation. A 10 μ L aliquot of this suspension was cast onto the surface of the pretreated GCE by using a microsyringe. The first modification layer was then air dried. Next, 15 μ L of chitosan acetate solution (20 mg of chitosan in 3 mL of 2% acetate solution, 30 min of ultrasonic agitation) was casted as the second modification layer. The electrode was air-dried, and the MOF-5-modified GCE (MOF-5–MGCE) was successfully fabricated.

2.4 Fabrication of the Au/MOF-5-composite electrode sensor and DNA detection

The DNA sensor was constructed with a sandwich-type configuration. The prepared MOF-5–MGCE was immersed in a solution containing 2 $\mu\text{mol}\cdot\text{L}^{-1}$ capture probe for 12 h for capture DNA adsorption. Then, the electrode was incubated in a complementary DNA solution (target DNA, 1 $\mu\text{mol}\cdot\text{L}^{-1}$) for 30 min. Capture DNA hybridized with the target DNA in accordance with complementary base-pairing rules. The electrode was washed and then incubated in the reporter probe (DNA-modified Au NP) solution for 30 min to allow the formation of a layer of particles on the MOF-5–MGCE surface.

3. RESULTS AND DISCUSSION

3.1 SEM

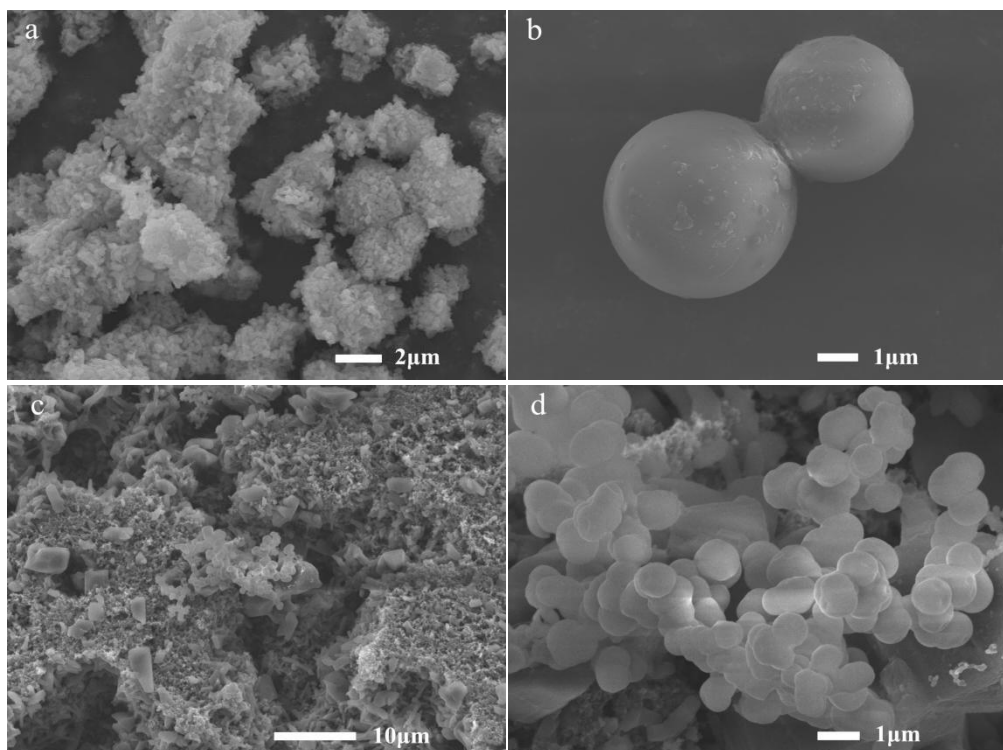


Figure 1. The SEM images of prepared MOF-5 (a,b) and the surface of MOF-5 modified glassy carbon electrode(c,d)

Figures 1a and 1b illustrate the morphology of the prepared MOF-5, which presents a uniform

spherical structure with a diameter of 2 μm . Figures 1c and 1d show the surface topography of the MOF-5–MGCE. Image c shows that the modified MOF-5 layer was composed of coarse particulate materials. The large number of spherical crystals shown in Figures 1d proves that MOF-5 crystals had been successfully modified on the GCE surface and that scattered MOF-5 crystals were connected by chitosan molecules. The outermost MOF-5 crystals were not wrapped in chitosan, and the characteristic structure of MOF-5 was not damaged. Chitosan acetate solution only functioned to ensure that MOF-5 was firmly fixed onto the surfaces of the GCE.

3.2 TEM images of Au NPs and DNA-modified Au NPs

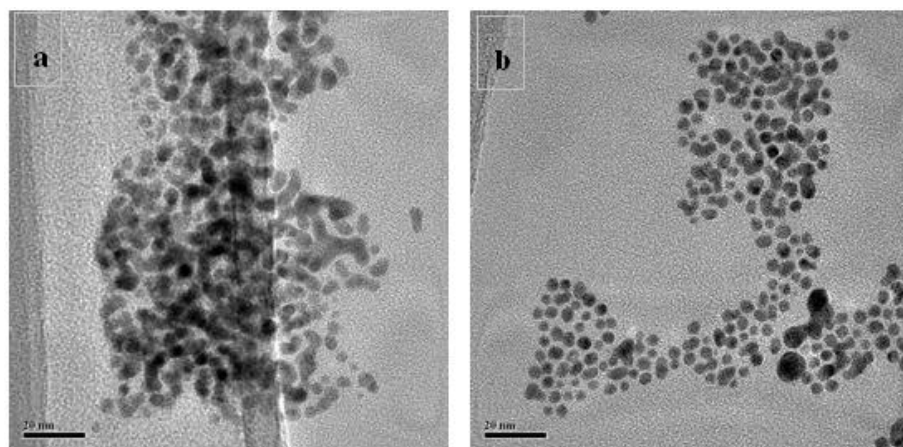


Figure 2. Representative TEM images of AuNPs (a), DNA modified AuNPs (b)

The TEM images of the prepared Au NPs are shown in Figure 2a. The images illustrate that the Au NPs were highly dispersed on the electrode without agglomeration. Au NPs exhibited a spherical structure and uniform particle diameters of 3–4 nm. These characteristics are consistent with the features inferred from the UV–vis absorption curve. The large surface areas and limited agglomeration of Au NPs with small particle sizes promoted catalytic activity during chemical reaction and are consistent with experimental requirements.

Comparing Figures 2a and 2b revealed that the particles of the newly prepared Au NP sol were densely packed, and the dispersibility of DNA-modified Au NPs was better than that of Au NPs. These characteristics may be attributed to the negative DNA charges that cause repulsion among DNA molecules[22] and indicate that DNA had been successfully modified onto Au NPs.

3.3 Analysis of electrocatalytic activity

Figure 3 presents a schematic of the three connection modes of the Au NP/DNA sensor to MOF-5–MGCE: (a) the direct combination of Au NPs with MOF-5–MGCE; (b) the combination of DNA-modified Au NPs with MOF-5–MGCE; and (c) the sequential combination of MOF-5–MGCE with Au NPs. The cyclic voltammetry (CV) curves of the MOF-5–MGCE bound to the Au NP/DNA sensor through each of these connections were acquired with an electrode voltage of 0.11 V and are shown in

Figure 3. The current of Au NP–MGCE was 1.503 μA , whereas that of MOF-5–MGCE was 18.23 μA . The current of MOF-5–MGCE was considerably higher than that of Au NP–MGCE. This characteristic illustrates that bare GCE adsorbed a low number of Au NPs. MOF-5 modification can drastically increase the number of Au NPs that adsorb on the electrode. It can also increase electrode conductivity and improve detection signal intensity.

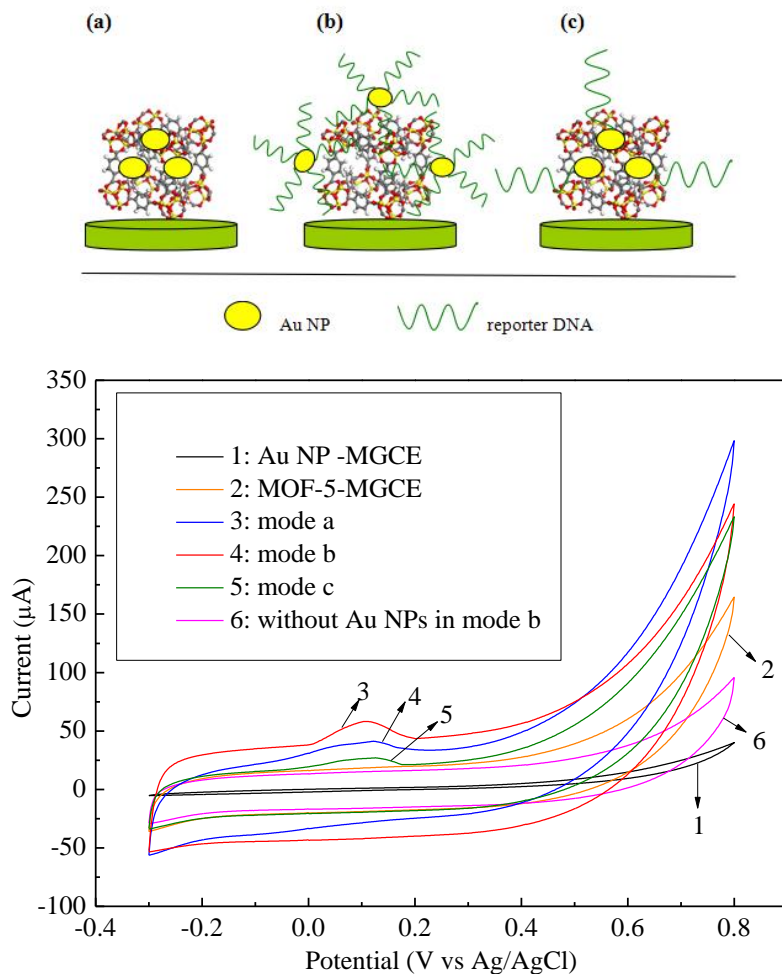


Figure 3. Three ways of connecting Au NPs and reporter DNA to MOF-5-MGCE, and the CV curves of different composite electrode.

MOF-5 exerted signal amplification effects. The electrocatalytic activity of MOF-5–MGCE that had been modified stepwise with the Au NP/DNA sensor (mode c) was lower than that of MOF-5–MGCE that had been modified with Au NPs (mode a). This result is consistent with a previous result showing that DNA modification inhibits the catalytic activity of Au NPs through electron tunneling, which is attributed to long distances between the electrode surface and Au NPs, and maximizes electrocatalytic activity[23]. The enhancement in the electrocatalytic activity of MOF-5 caused by modification with the Au NP/DNA sensor was better than that caused by modification with Au NPs alone because of the porous structure of MOF-5. Specifically, as shown in Figure 5S in the Supporting Information section, the BET specific surface area of MOF-5 was $914.7 \text{ m}^2 \cdot \text{g}^{-1}$. The diameters of Au

NPs ranged from 3–4 nm, whereas those of MOFs ranged from 2–50 nm. Au NPs mainly adsorbed onto the inner walls of MOF-5 pores in the Au NP-modified MOF-5–MGCE such that the number of Au NPs that adsorbed onto the surfaces of the material decreased. The number of Au NPs that adsorbed in MOF-5 pores drastically reduced when Au bound with detection DNA chains because DNA strands have a certain length. The reduction in Au NP adsorption in pores can mitigate the effects of electron tunneling caused by the long distances between the electrode surface and Au NPs and can maximize electrocatalytic activity. This finding also accounts for the highest electrocatalytic activity shown by binding mode (b) among the studied modes.

Only the CV curves of electrodes containing Au NPs had oxidation peaks. This result illustrates that Au NPs are the only electrocatalytic active substances for hydrazine electro-oxidation[24] with a key function in electrochemical signal amplification and may be used as signal labels for electrocatalytic activity[25,26]. Moreover, MOF-5–MGCE that had been surface-modified with Au NPs had the highest electro-oxidation activity. Low electron transfer power and electron tunneling can produce high overpotentials, which influence the oxidation of hydrazine and decrease the current intensities of DNA biosensor systems. Comparing the three connection modes of the Au NP/DNA sensor with those of MOF-5–MGCE showed that mode b had the highest oxidation peak current and that the oxidation potential followed the order of b < a < c. The CV curves of mode b without Au NPs lacked an oxidation peak. The current of mode b was slightly lower than that of MOF-5–MGCE. This result indicates that electron transfer power rapidly increased, system over-potential was attenuated, and oxidation was promoted only when Au NPs were used in the DNA sensor. These effects intensified when Au NPs adsorbed on the surface of MOF-5. MOF-5 presented electrochemical signal amplification effects. Moreover, the pores on MOF-5 increased the probability of hydrogen adsorption onto Au NPs and formed an enhanced active region that can provide the driving forces that accelerate electron transfer for hydrazine electro-oxidation on Au NPs[27]. The frame structure of MOF-5 overcame the electron tunneling effect caused by the long distance between the electrode surface and Au NPs and maximized electrocatalytic activity.

3.4 Electrochemical behavior of the electrochemical DNA biosensor

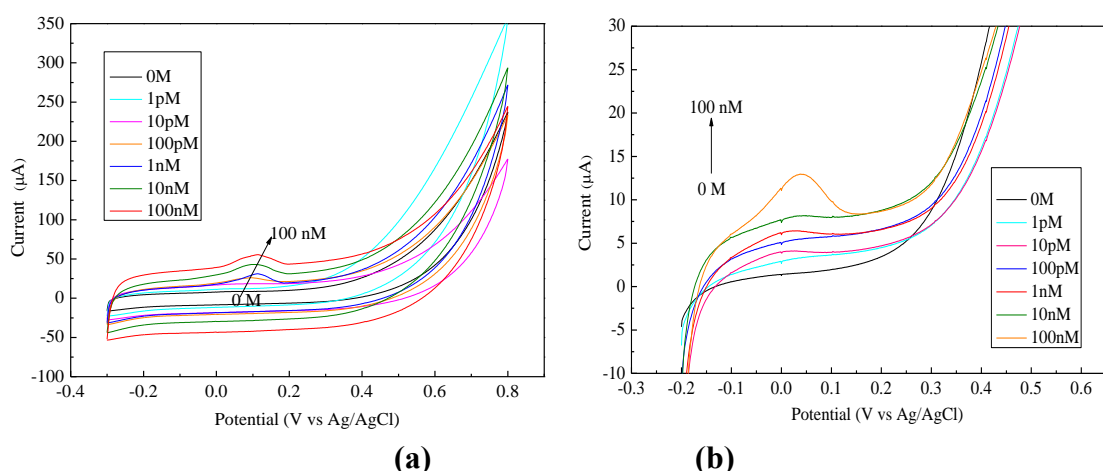


Figure 4. The CV (a) and LSV (b) curves of prepared electrochemical DNA sensor.

Figure 4a shows the CV results obtained with different target DNA concentrations. The peak shift increased as the target DNA concentration was increased. Au NPs that had adsorbed onto MOF-5–MGCE presented electrocatalytic activity during hydrazine oxidation. This behavior indicates that the number of Au NPs increased with increasing target DNA concentration. Thus, Au NPs can be widely used as electrochemical sensing signal labels in DNA biosensors[28]. The current at 0.1 V was 8.660 and 12.49 μ A when the target DNA concentration was 0 M and 1 pM, respectively. In addition, the widths of the CV curves increased, and the intensity of the oxidation peak strengthened. Target DNA at concentrations of 1 pM can be accurately detected by using the method developed in this work.

Metal NPs rendered changes in electrical signals in the CV scans undetectable by preventing the over-potential near the electrode from changing when the target DNA concentration was less than 100 pM[29]. However, the CV curves obtained in the present study indicate that electrical changes can be detected at low target DNA concentrations by considering the electrocatalytic activity of Au NPs as signal amplification labels and enhancing this activity through connection with modified MOF-5. The prepared electrochemical DNA sensor thus showed high sensitivity.

The LSV results for the DNA sensor in the presence of different target DNA concentrations are shown in Figure 4b and were consistent with CV results. The electrocatalytic current increased with the increase in target DNA concentration, and the start potential of the oxidation reaction shifted toward less positive values. The nonspecific binding of the negative-end phosphate of the DNA chain with an organic amine can intensify the background signal and can be reduced by the conversion of unreacted organic amines to anhydrides under the electrochemical effect[30]. As shown in Figure 4b, the current of the sensor in the absence of target DNA was considerably lower than that in the presence of 1 pM target DNA. This result indicates that nonspecific binding is unlikely to occur upon DNA detection.

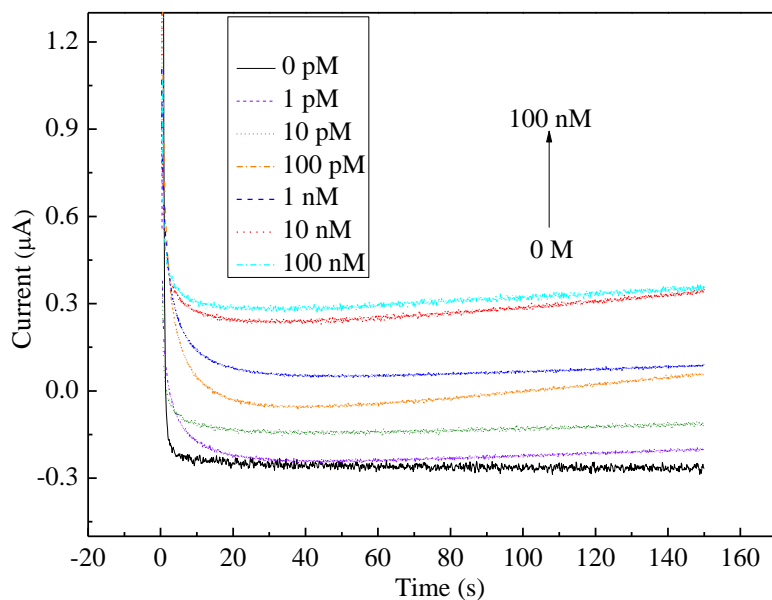


Figure 5. The Chronoamperometry curves of prepared electrochemical DNA sensor.

The chronoamperometry curves of the electrochemical DNA biosensor are presented in Figure

5. The curves show that the electrocatalytic oxidation current increased as the target DNA concentration was increased. The slow increment in current with the prolongation of the reaction time indicates that the reactivity of electrocatalytic oxidation mainly remained constant and only slightly increased under the given conditions. The current demonstrates an approximate staircase response when the target DNA concentration was 1 pM. Certain differences in peak shape and height that may be associated with the shapes and sizes of Au NPs that had adsorbed onto the surfaces of the MOF-5-modified electrode remained. The overall trend was regular and reflected the electrocatalytic mechanism of Au NPs and the MOF-5 material during oxidation. The NPs can catalyze hydrazine oxidation. The current increased upon the instantaneous adsorption of Au NPs onto the surfaces of the MOF-5–MGCE. However, the instantaneous current decayed back to its original values when the NPs were located far from the surfaces of MOF-5–MGCE.

Transient current spikes appeared only at extremely low target DNA concentrations given the potential effect of background current. The background current in the presence of high target DNA concentrations was sufficiently high such that distinguishing the current step from the background level was difficult. Therefore, the curves obtained in the presence of other DNA concentrations were smoother than those obtained in the presence of 1 pM DNA. Chronoamperometry can accurately detect current changes at extremely low target DNA concentrations, such as 1 pM.

3.5 Determination of the detection limit of the electrochemical DNA biosensor

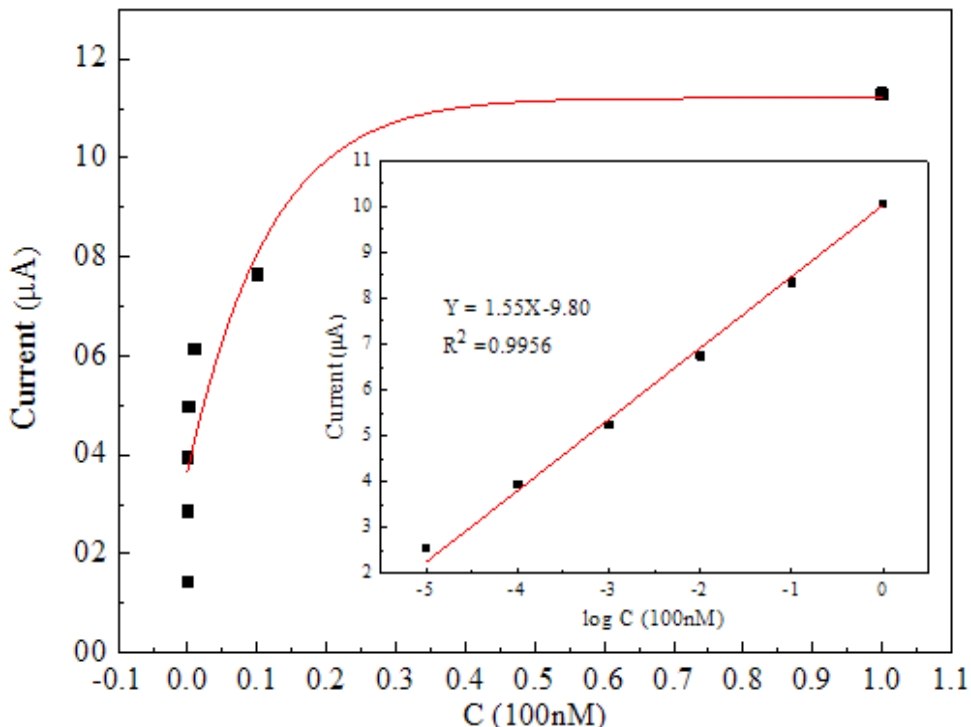


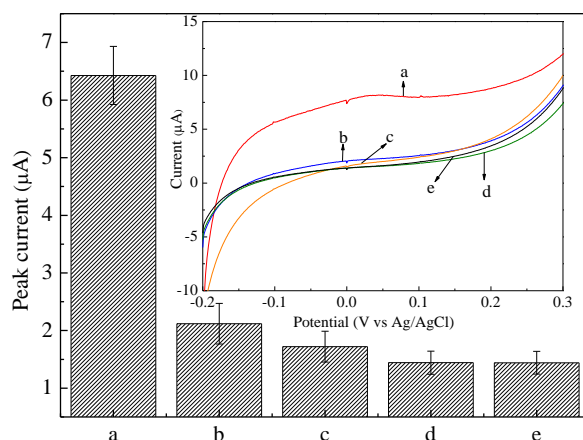
Figure 6. The relationship between anodic peak current and concentration of target DNA.

Table 1. Comparison of the analytical performance of electrochemical biosensors that use nanoparticles as electrocatalysts for signal amplification.

Nanoparticle label	Analyte	Dynamic range	LOD	Ref.
Au	Human serum albumin	0.5-200 μ g mL ⁻¹	1ng mL ⁻¹	31
Au	Human IgG	0.01-10 ng mL ⁻¹	9pg mL ⁻¹	32
AuNPs-PAT/rGO	DNA	0.5-400pM	0.06pM	33
ferrocene-capped Au NPs	ApoE 4 gene	0.1-100pM	0.1 pM	34
Co-MOFs/PtPdNPs	DNA	1pM-30nM	0.32pM	35
Au Nanoparticle /MOF-5	DNA	1pM-100nM	0.05pM	Our Work

Target DNA can be accurately detected at concentrations of 1 pM to 100 nM. The peak currents of the LSV curves for different target DNA concentrations were selected to construct a standard curve and determine the relationship between peak current and target DNA concentration (Figure 6). The current was 2.862 μ A at a target DNA concentration of 1 pM and was significantly higher than that at the target DNA concentration of 0 pM (1.424 μ A). Hence, the logarithmic of target DNA concentrations of 1 pM to 100 nM presented a good linear relationship with current. The equation representing the linear relationship between current intensity and $\log C$ ($C / 100$ nM) is $Y = 1.55X - 9.8$. This equation was used to calculate the minimum detection limit. The minimum detection limit was calculated as 0.05 pM, which was considerably lower than previously reported values (e.g., 3 and 1.3 nM)[19]. As shown in Table 1, Compared the analytical performance with other materials, such as Au[31, 32], AuNPs-PAT/rGO[33], ferrocene-capped Au NPs[34] and Co-MOFs/PtPdNPs[35], Au Nanoparticle/MOF-5 has the lowest detection limit, which illustrate that MOF-5 can drastically improve the biosensor detection limit when used to construct DNA biosensors by intensifying the detection signal.

3.6 Selectivity of the electrochemical DNA biosensor

**Figure 7.** The comparison of the peak current of prepared electrochemical DNA sensor hybridized with target DNA (a), one base-mismatched DNA (b), three base-mismatched DNA (c), non-complementary DNA (d) and only the hybridization buffer containing no DNA sequences (e)

Control experiments were performed by hybridizing different DNA sequences with Au NPs modified with 10 nm detection DNA to confirm the selectivity of the electrochemical DNA biosensor. These sequences included a complementary DNA sequence, a base-mismatched DNA sequence, three base-mismatched DNA sequences, and a noncomplementary DNA sequence. As shown in Figure 7, the noncomplementary DNA sequence produced a negligible peak current (signal d) that was similar to the background signal (signal e). The three base-mismatched DNA produced a weak peak current (signal c) and the base-mismatched DNA generated a quarter peak current (signal b) when compared with the complementary sequence (signal a). The sequence specificity of the detection-DNA-modified Au NPs may be mainly attributed to the intrinsic recognition ability of DNA bases[36,37]. Moreover, the noncomplementary and base-mismatched DNA cannot complementarily pair with the detection-DNA-modified Au NPs and cannot produce the electro-oxidation signal. Hence, the prepared electrochemical sensor has good selectivity.

4. CONCLUSION

In this paper, We successfully prepared a Au/MOF-5 composite electrode electrochemical DNA sensor for detecting trace amounts of DNA. Au NPs with large specific surface areas exhibited high electrocatalytic activity for hydrazine electro-oxidation. The unique structural features of MOF-5 can overcome the low electron transfer power and electron tunneling presented by DNA-modified Au NPs. The unique porous structure of MOF-5 drastically enhanced the electrocatalytic activity of the Au NPs and improved the DNA detection limit. Signal strength and limit considerably improved through the combination of Au NPs and MOF.

SUPPORTING INFORMATION

MOF-5(IL): electrochemical synthesis MOF-5 in ionic liquid

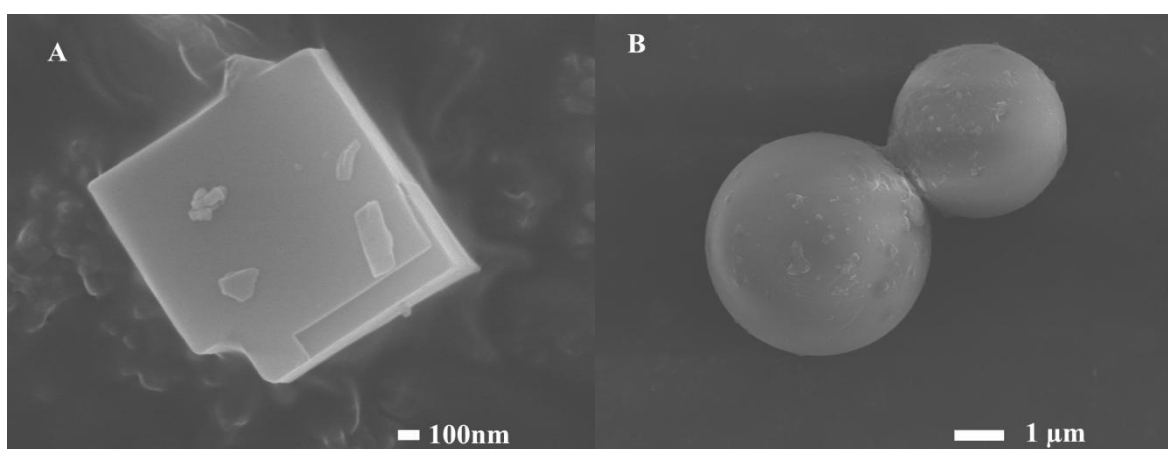


Figure 1S. The SEM images of MOF-5 prepared by Huang's method (A) and MOF-5 (IL) (B)

MOF-5, synthesised by the conventional method, presents a regular cubic structure of 1 μ m, whereas MOF-5 (IL), synthesised by electrochemical method in the Bmim chloride, shows a spherical

morphology with a 3 μm diameter (Figure 1S). The comparison of two images illustrates that the differences in the synthetic methods greatly influences the morphology of the material. With electrochemical energy, the conventional cubic configuration of MOF-5 is distorted significantly. Changes in the orientation of Zn^{2+} and BDC^{2-} can result from the directional movement of ions due to the applied electric field. Thus, the use of electric current during the synthesis of MOFs can generate newer configurations of anions and cations inaccessible by other synthetic methods. Meanwhile, the ionic liquid, Bmim chloride, also plays an important role towards the distinct calabash-shaped morphology. The cations of ionic liquids often function as templates and direct the structure of the framework. However, the optimal concentration of the ionic liquid has to be determined. Higher concentrations of the ionic liquid will lead to a decrease in the conductivity of the solution, reducing the influence of the current on morphology of synthesised MOFs.

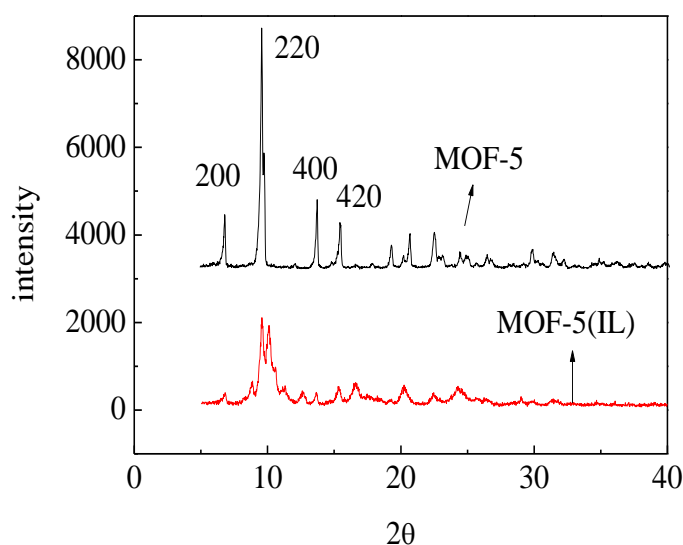


Figure 2S. The XRD spectra of MOF-5 (IL)

The XRD pattern of MOF-5(IL) is very similar to that of MOF-5 (Figure 2S). The overlap of the four main peaks (6.8° , 9.7° , 13.7° and 15.4°) illustrates that MOF-5 can be successfully prepared in an ionic liquid through electrochemical method. The sharp spike confirms the crystallinity of the product. In contrast to the spectra of MOF-5, there is a distinct split at 9.7° in the spectra of MOF-5(IL). This split is the likely result of the distortion in conventional cubic symmetry structure, which is consistent with SEM images that show a calabash structure for MOF-5(IL). The peaks at 31.5° , 34.6° and 36.1° in the spectra of MOF-5 show the presence of trace amounts of ZnO . There is no spectral evidence for presence of ZnO in MOF-5 (IL). These observations indicate that electrochemical synthesis in ionic liquids generates MOFs with higher purity than that prepared through conventional methods.

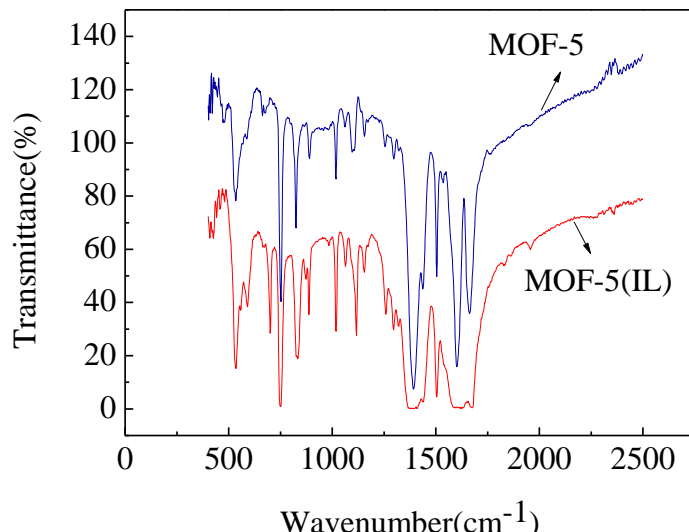


Figure 3S. The infrared spectra of MOF-5 and MOF-5 (IL)

The FTIR spectra of MOF-5 and MOF-5(IL) are shown in Figure 3S. Irrespective of the peak shape and wave numbers, the similarity of the two spectra illustrates that MOF-5 can be successfully synthesised by electrochemical method in ionic liquids. Peaks at 1501 cm^{-1} and 1588 cm^{-1} are due to the asymmetric stretching, while that at 1388 cm^{-1} is due to symmetrical stretching vibration of carboxylic acid groups in BDC. The peak at 1640 cm^{-1} can be ascribed to hydroxyl group (moisture in KBr pellets). Peaks in $1284\text{--}730\text{ cm}^{-1}$ range can be attributed to the in-plane vibrations of BDC. The 1,4-substitution pattern of the phenyl ring is highlighted by two out-of-plane aromatic C–H bending peaks ($800\text{--}750\text{ cm}^{-1}$). The slight differences in the peak shape and intensity (with same wave number) is mainly due to the differences in the reaction conditions (temperature, solvent, reaction time, current density and so on).

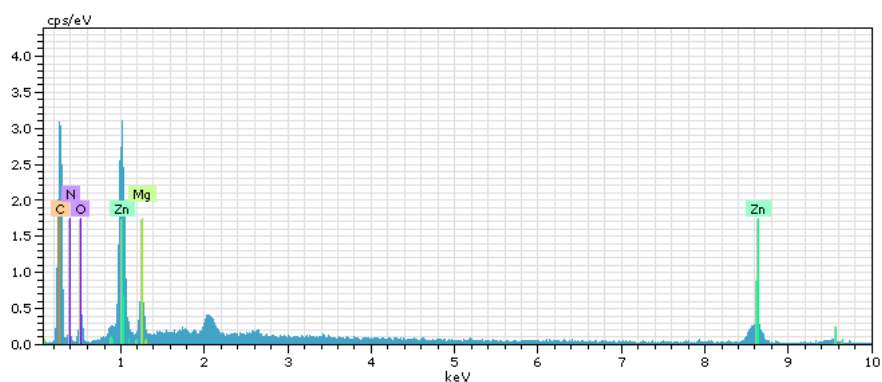


Figure 4S. the EDS spectrum diagram of MOF - 5 (IL)

Analysis of the EDS spectrum reveals the components of MOF-5(IL) as C (72.27%), Zn (9.96%), O (7.28%) and N (1.14%) (Figure 4S). When compared with MOF-5 (reported formula = $\text{Zn}_4\text{O}_{13}\text{C}_{24}\text{H}_{12}$), the content of C atoms in MOF-5(IL) is 26.99% higher. The likely explanation for this is that some small solvent molecules remain adsorbed in the holes of MOF-5(IL). This can be further confirmed on analysis of the EDS spectrum of MOF-5(IL), which contains a certain amount of N atoms.

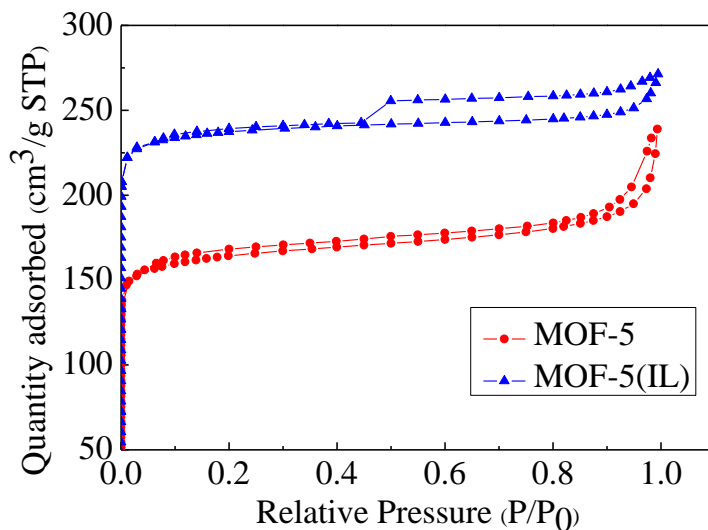


Figure 5S. Nitrogen adsorption and desorption isotherms of MOF-5 and MOF-5(IL)

From the nitrogen adsorption and desorption isotherms (Figure 5S.) we can get that the BET specific surface area of MOF-5 and MOF-5(IL) was $627.3 \text{ m}^2\cdot\text{g}^{-1}$ and $914.7 \text{ m}^2\cdot\text{g}^{-1}$, respectively. The isotherms of MOF-5 is typical I type adsorption curve, but MOF-5(IL) belongs to IV type adsorption curve. It illustrated that electrochemical synthesis method could not destroy the porosity of MOFs material, it can keep the complete pore structure of MOFs and improve its specific surface area.

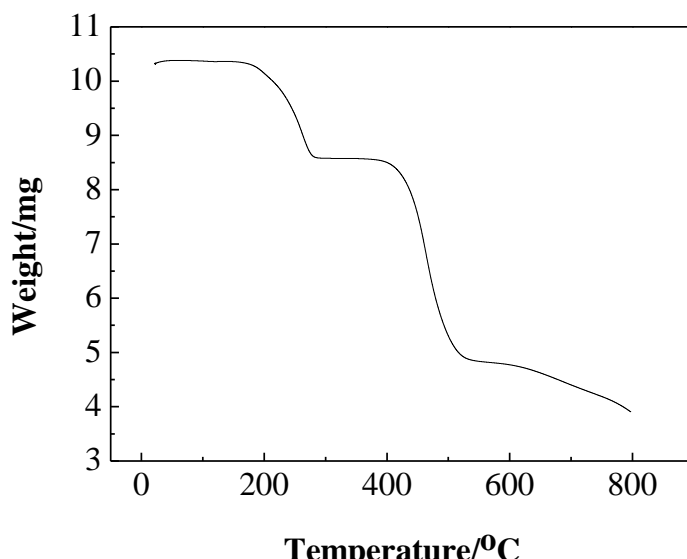


Figure 6S. The TG curve of MOF-5(IL)

The TG curve of MOF-5(IL) displays two obvious weight loss processes (Figure 6S). The first loss in mass occurs at 190–295 °C while the second loss is observed in 380–580 °C range. The loss in mass (~16.5%) during the first process can be attributed to the release of small molecules that are adsorbed in the holes of MOF-5(IL). The larger decline in mass (35.6%) after 380 °C is mainly due to disruption in the skeleton of MOF-5 (IL) and its decomposition at high temperature. Above 540 °C, the weight of sample is essentially unchanged, with the final product being ZnO.

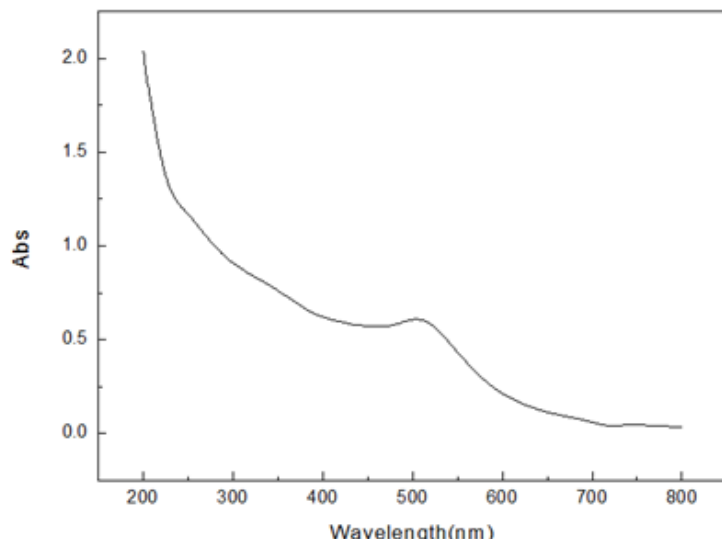


Figure 7S. UV-visible absorption curve of gold nanoparticles

The UV-vis spectra of the prepared Au NPs shown in Figure 7S demonstrate that the absorption peak of the NPs occurs at 504 nm and that the maximum absorbance is 0.54. These findings meet the experimental requirements.

ACKNOWLEDGEMENTS

This work was supported by National Foundation of China (Grant No.51703151) and the applied basic research project of Shanxi province (Grant No.201601D011023). The authors sincerely thanks for anonymous reviewers for their valuable comments.

References

1. N.X. Li, M.Y. Du, Y.C. Liu, X.H. Ji, Z.K. He, *ACS Sensors*, 3(2018)1283.
2. X.M. Shi, G.C. Fan., X.Y. Tang, Q.M. Shen, J.J. Zhu, *Biosens. Bioelectron.*, 109(2018)190.
3. L. Zou, T.T. Li, R.D. Shen, S.Z. Ren, L.S. Ling, *Talanta*, 189(2018)137.
4. A. Banasiak, J. Cassidy, J. Colleran, *Biosens. Bioelectron.*, 117(2018)217.
5. A. Patterson, F. Caprio, A. Vallee-Belisle, D. Moscone, K.W. Plaxco, G. Palleschi F., Ricci, *Anal. Chem.*, 82(2010) 9109.
6. B. Kaur, K. Malecka, D.A. Cristaldi, C.S. Chay, I. Mames, H. Radecka, J. Radecki, E. Stulz, *Chem. Commun.*, 54(2018)11108.
7. H.R.A. Hasanjani, K. Zarei, *Biosens. Bioelectron.*, 128(2019)1.
8. Y.G. Sun, X.X. He, J. Ji, M. Jia, Z.P. Wang, X.L. Sun, *Talanta*, 141(2015)300.
9. X.L. Zhu, Y.X. Liu, J.H. Yang, Z.Q. Liang, G.X. Li, *Biosens. Bioelectron.*, 25(2010)2135.
10. S.J. Kwon, F.R.F. Fan, A.J. Bard, *J. Am. Chem. Soc.*, 132(2010)13165.
11. H. Kim, S. Yang, S.R. Rao, S. Narayanan, E.A. Kapustin, H. Furukawa, A.S. Umans, O.M. Yaghi, E.N. Wang, *Science*, 2017, 356 (6336), 430-434.
12. X.L. Cui, K.J. Chen, H.B. Xing, O.W. Yang, R. Krishna, Z.B. Bao, H. Wu, W. Zhou, X.L. Dong, Y. Han, B. Li, O.L. Ren, M.J. Zaworotko, B.L. Chen, *Science*, 353(2016)141.
13. L.J. Zhang, Y.Y. Zhang, S.L. Huang, Y.L. Yuan, H. Li, Z.Y. Jin, J.H. Wu, Q.F. Liao, L. Hu, J.G. Lu, *Electrochim. Acta*, 281(2018)189.
14. Y.L. Liu, X.J. Zhao, X.X. Yang, Y.F. Li, *Analyst*, 138(2013)4526.

15. X.M. Hai, N. Li, K. Wang, Z.Q. Zhang, J. Zhang, F.Q. Dang, *Anal. Chim. Acta*, 998(2018)60.
16. J.F. Guo, C.M. Li, X.L. Hu, C.Z. Huang, Y.F. Li, *RSC Adv.*, 4(2014)9379.
17. L.F. Chen, H.Y. Zheng, X. Zhu, Z.Y. Lin, L.H. Guo, B. Qiu, G.N. Chen, Z.N. Chen, *Analyst*, 138(2013)3490.
18. X. Zhu, H.Y. Zheng, X.F. Wei, Z.Y. Lin, L.H. Guo, B. Qiu, G.N. Chen, *Chem. Commun.*, 49(2013)1276.
19. Y.J. Cui, Y.F. Yue, G.D. Qian, B.L. Chen, *Chem. Rev.*, 112(2012)1126.
20. X.L. Zhu, H.H. Zhang, C. Feng, Z.H. Ye, G.X. Li, *RSC Adv.*, 4(2014)2421.
21. H.M. Yang, X.L. Song, T.L. Yang, Z.H. Liang, C.M. Fan, X.G. Hao, *RSC Adv.*, 4(2014)15720.
22. S. Cinti, E. Proietti, F. Casotto, D. Moscone, F. Arduini, *Anal. Chem.*, 90(2018)13680.
23. X.M. Meng, M.R. Xu, J.Y. Zhu, H.S. Yin, S.Y. Ai, *Electrochim. Acta*, 71(2012)233.
24. P. Bansal, G. Bhanjana, N. Prabhakar, J.S. Dhau, G.R. Chaudhary, *J. Mol. Liq.*, 248(2017)651.
25. X.L. Liu, Z.Y. Yang, Q.L. Sheng, J.B. Zheng, *J. Electrochem. Soc.*, 165(2018)B596.
26. Y.X. Ma, A.L. Highsmith, C.M. Hill, S.L. Pan, *J. Phys. Chem. C*, 122(2018)18603.
27. N. Roy, K. Bhunia, C. Terashima, A. Fujishima, D. Pradhan, *ACS Omega*, 2(2017)1215.
28. H.B. Pu, X.H. Xie, D.W. Sun, Q.Y. Wei, Y.F. Jiang, *Talanta*, 195(2019)419.
29. Y. Qian, D.Q. Tang, L.L. Du, Y.Z. Zhang, L.X. Zhang, F.L. Gao, *Biosens. Bioelectron.*, 64(2015)177.
30. S.J. Kwon, A.J. Bard, *J. Am. Chem. Soc.*, 134(2012)10777.
31. K. Omidfar, H. Zarei, F. Gholizadeh, B. Larijani, *Anal. Biochem.* 421 (2012) 649.
32. 32.Q.N. Xu, F. Yan, J.P. Lei, C. Leng, H.X. Ju, *Chem. A Eur. J.* 18 (2012) 49.
33. M.B. Gholivand, A. Akbari, *Biosens. Bioelectron.*, 129(2019)182.
34. H.W. Lu, L. Wu, J.R. Wang, Z.X. Wang, X.Y. Yi, J.X. Wang, N. Wang, *Microchim. Acta*, 185(2018)549.
35. Yang, X ; Lv, JJ ; Yang, ZH; Yuan, R; Chai, YQ , *Anal. Chem.*, 89(2017)11636.
36. Y.C. Yang, C. Li, L. Yin, M.Y. Liu, Z.X. Wang, Y.Q. Shu, G.X. Li, *ACS Appl. Mater. Inter.*, 6(2014)7579.
37. H.F. Cui, L. Cheng, J. Zhang, R.H. Liu, C. Zhang, H. Fan, *Biosens. Bioelectron.*, 56(2014)124-128.